Preparation of nanocrystalline LiMnPO$_4$ via a simple and novel method and its isothermal kinetics of crystallization

Chen Liu · Xuehang Wu · Wenwei Wu · Jinchao Cai · Sen Liao

Abstract The precursor of nanocrystalline LiMnPO$_4$ was obtained by solid-state reaction at low heat using Li$_2$SO$_4$·H$_2$O, MnSO$_4$·H$_2$O, and Na$_3$PO$_4$·12H$_2$O as raw materials, maintaining the mixture at 333 K for 4 h, and then washing the mixture with deionized water to remove soluble inorganic salts, and at last drying at 373 K. The nanocrystalline LiMnPO$_4$ was obtained by calcining the precursor. The precursor and its calcined products were characterized using TG/DTA, FT-IR, and XRD. The data showed that the precursor dried at 373 K for 3 h was a compound with amorphous structure. However, when the precursor was calcined at 973 K for 2 h, highly crystallization LiMnPO$_4$ with orthorhombic structure [space group Pmnb (62)] was obtained with a crystallite size of 38 nm. The mechanism and kinetics of the crystallization process of LiMnPO$_4$ were studied using XRD technique, the results showed that activation energy of the crystallization process of LiMnPO$_4$ was 103.30 kJ/mol, and the mechanism of crystallization process of LiMnPO$_4$ is the random nucleation and growth of nuclei reaction.

Introduction

It is well known that the cathode materials in rechargeable Li-ion batteries commercially used are the layered rock salt oxides, such as Li$_x$CoO$_2$, Li$_x$NiO$_2$, Li$_x$Mn$_2$O$_4$, Li$_x$Ni$_{0.8}$Co$_{0.2}$O$_2$, Li$_x$(Ni$_{0.8}$Co$_{0.15}$Al$_{0.05}$)O$_2$, and Li$_y$[Ni$_x$Co$_{1-2x}$Mn$_x$]O$_2$. However, these oxides are unstable and can decompose and release O$_2$ at elevated temperatures [1–5]. The released O$_2$ can ignite the organic solvents in the electrolyte and create hazardous conditions including fire and explosion. Recently, olivine-type LiMPO$_4$ (M = Fe, Mn, Co, and Ni) compounds have been promoted as safe alternative cathode materials for lithium-ion batteries, which is attributed to its excellent recyclability, thermal stability, low-cost, and environmental benefits.

Since LiFePO$_4$ was proposed by Padhi et al. in 1997 [6], various methods have been developed to synthesize nanocrystalline LiMnPO$_4$ compounds, including solid-state reaction [7–10], sol-gel technique [11, 12], polyol method [13, 14], hydrothermal method [15], spray pyrolysis [16, 17], precipitation method [18], etc. The rate capability of LiMnPO$_4$ compounds can be improved by many methods, such as to form well dispersed and small particles as well as to coat them with conductive materials [19–22]. Yamada et al. confirmed that Li(Mn$_x$Fe$_{1-x}$)PO$_4$ (0.6 < x < 0.8) samples would be useful in the coexistence of the 3.4 and 4.1 V [23]. Delacourt et al. [24] observed a reversible capacity of about 70 mAh/g and of about 140 mAh/g in the Li/LiMnPO$_4$ cell, respectively. Oh et al. [17] obtained a discharge capacity of 158 mAh/g at 1/20 C, 126 mAh/g at 1 C, and 107 mAh/g at 2 C rate.

Different raw materials and synthesis methods will result in different electrochemical properties of LiMnPO$_4$ associated with the crystallization temperature, crystallite size, and morphology. Therefore, new synthesis methods for LiMnPO$_4$ still need to be studied and innovated further. Besides, the mechanism and kinetics studies of crystallization for LiMnPO$_4$ are needed to obtain high-performance lithium metal phosphates cathode materials for practical applications.

C. Liu · X. Wu · W. Wu (✉) · J. Cai · S. Liao
School of Chemistry and Chemical Engineering, Guangxi University, Nanning 530004, China
e-mail: gxuwuwenwei@yahoo.com.cn

C. Liu
Guangxi Institute of Metallurgy, Nanning 530023, China

In this article, olivine-type LiMnPO$_4$ was synthesized via solid-state reaction at low heat [25], and the mechanism of crystallization, and kinetics of the crystallization process of LiMnPO$_4$ were investigated for the first time. Isothermal kinetics of the crystallization process of LiMnPO$_4$ could be described by JMA equation [26–28]. Avrami exponent, n, was used to estimate mechanism of crystallization process.

Experimental

Synthesis

Nanocrystalline LiMnPO$_4$ has been synthesized by solid-state reaction at low heat using Li$_2$SO$_4$·H$_2$O, MnSO$_4$·H$_2$O, and Na$_3$PO$_4$·12H$_2$O as starting materials. All chemical reagents used were of high purity. The raw materials were mixed in a Li$_2$SO$_4$·H$_2$O:MnSO$_4$·H$_2$O:Na$_3$PO$_4$·12H$_2$O molar ratio of 0.5:1:1.15. The mixture was fully ground in a mortar with a rubbing mallet for 40 min in the presence of surfactant polyethylene glycol (PEG)-400 at first, and then the mixture was kept at 333 K for 4 h. The mixture was washed with deionized water to remove soluble inorganic salts until SO$_4^{2-}$ ion could not be visually detected by a 0.5 mol/L BaCl$_2$ solution. The precipitate was then washed with a small amount of anhydrous ethanol and dried at 373 K for 3 h. Nanocrystalline LiMnPO$_4$ was obtained via calcining precursor above 973 K for 2 h.

Characterization

Thermogravimetry and differential thermal analyses (TG/DTA) measurements were made using a Netsch 40PC thermogravimetric analyzer. X-ray powder diffraction (XRD) was performed using a Rigaku D/max 2500 V diffractometer equipped with a graphite monochromator and a Cu target. FT-IR spectra of the precursor and its calcined product were recorded on a Nexus 470 FT-IR instrument.

Kinetics of crystallization process

Isothermal crystallization of LiMnPO$_4$ could be described by JMA equation [26–29].

$$x = 1 - \exp[-(kt)^n]. \tag{1}$$

The double logarithm equation of Eq. 1 can be written in the Eq. 2:

$$\ln[-\ln(1 - \chi)] = \ln k + n \ln t, \tag{2}$$

where χ is the crystallized fraction of LiMnPO$_4$ at a given temperature time t, k is the rate constant of crystallization, and n is the Avrami exponent that is related to the

crystallization mechanisms. The dependence of $\ln(-\ln(1-\chi))$ on $\ln t$ must give rise to a straight line. Thus, the Avrami exponent (n) can be obtained from linear slope (that is: linear slope $= n$), and the rate constant (k) of crystallization can be obtained from linear intercept ($h = \ln k$).

The dependence of the rate constant (k) on the effective activation energy, E_c, can be expressed in Arrhenius equation (Eq. 3).

$$k = k_0 \exp\left(\frac{-E_c}{RT}\right), \tag{3}$$

where k is the rate constant of crystallization, E_c is the effective activation energy (kJ/mol), k_0 is the pre-exponential factor, R is the gas constant (8.314×10^{-3} J mol^{-1} K^{-1}), and T is reaction temperature (K).

By a series of transforms, thus Eq. 3 can be rewritten in the Eq. 4:

$$E_c = R\left(\ln\frac{k_2}{k_1}\right)\left(\frac{T_1 T_2}{T_2 - T_1}\right). \tag{4}$$

k_2 and k_1 are the rate constants of crystallization corresponding to reaction temperature T_1 and T_2, respectively. Thus, the effective activation energy (E_c) of the crystallization process of LiMnPO$_4$ can be obtained according to Eq. 4.

Results and discussion

Figure 1 showed the TG/DTA curves of the precursor at a heating rate of 10 K/min from ambient temperature to 1173 K.

The TG/DTA curves show that thermal decomposition of the precursor below 1173 K occurs in only a well-defined step, which starts at about 303 K, ends at about 873 K, and characterized by a strong endothermic DTA peak at about 446 K that can be attributed to the dehydration of adsorbed
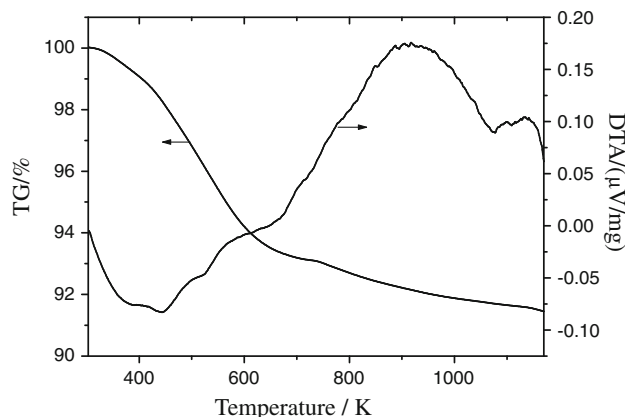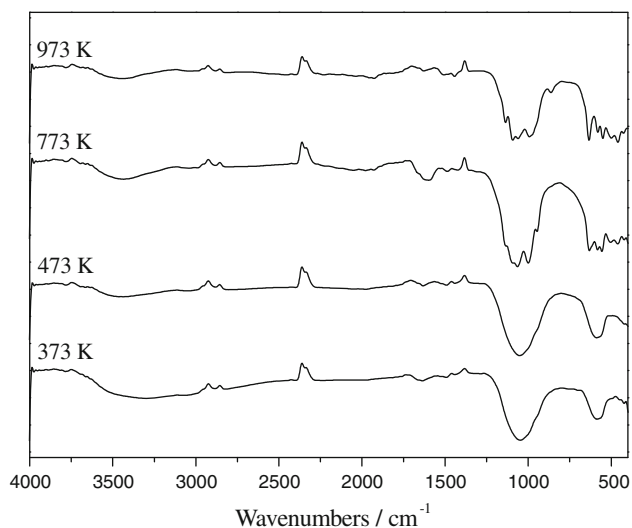

Fig. 1 TG/DTA curves of LiMnPO$_4$ precursor

water and crystal water from the precursor. The observed mass loss in the TG curve between 303 and 873 K is 7.68%. The broad exothermic DTA peak at about 918 K can be attributed to the phase change from amorphous $LiMnPO_4$ to orthorhombic $LiMnPO_4$ [26–29].

The FT-IR spectra of the precursor and calcined samples are shown in Fig. 2. The strong bands at 1150–900 cm^{-1} are attributed to the P–O stretching vibrations. The bending OPO vibrations appear in the region of 650–500 cm^{-1}. The weak band at about 726 cm^{-1} is the water libration (hindered rotation), while the strong and broad band at about 3400 cm^{-1} is assigned to the stretching OH vibration of the water molecule [30, 31]. The weak bands, which appear at 1631 and 1493 cm^{-1} in the spectrum of the precursor, can be ascribed to the bending mode of the HOH [32, 33]. The bands of calcined samples above 473 K, which are located at 726, 1493, 1631, and 3400 cm^{-1}, are attributed to the adsorbed water for air. FT-IR spectra of the two samples obtained at 373 and 473 K are similar. However, the two spectra have a great difference in comparison with that of calcined samples above 773 K. Such as, the band of the calcined samples above 773 K at about 1049 cm^{-1} is split into three bands at 993, 1073, and 1141 cm^{-1}, and the band at about 580 cm^{-1} is split into two bands at 556 and 637 cm^{-1} when the precursor sample was calcined above 773 K, which indicates the structure of the calcined samples above 773 K takes place transform.

Figure 3 shows the XRD patterns of the precursor and its calcined products for 2 h. The results show that the precursor dried at 373 K was a compound with amorphous structure. When the precursor was calcined at 773 K for 2 h, a characteristic diffraction pattern of crystal is observed. This indicates that the calcined product obtained at 773 K for 2 h is crystalline. However, diffraction peaks
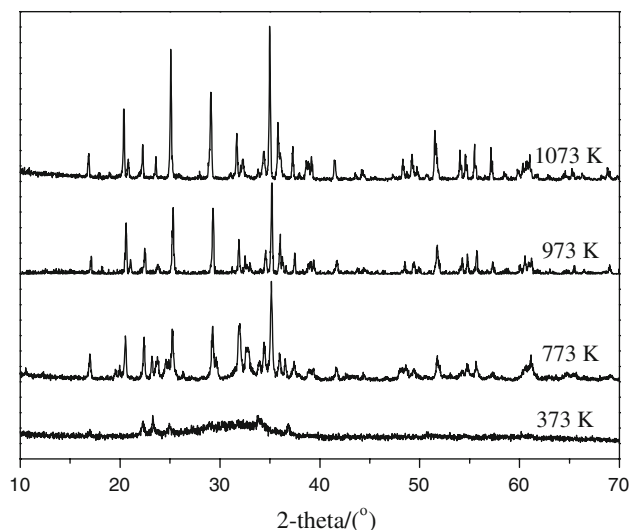

Fig. 3 XRD patterns of the products obtained at different calcined temperatures for 2 h

of other impurities, such as $Mn_3(PO_4)_2$ and Mn_2O_3 are still observed. All the diffraction peaks in the pattern of samples obtained above 973 K are in agreement with that of orthorhombic $LiMnPO_4$, with space group Pmnb (62), lattice parameter $a = 6.100$ Å, $b = 10.460$ Å, $c = 4.744$ Å, $\alpha = \beta = \gamma = 90°$, Density = 3.5305 g/cm^3, from PDF card 74-0375. Intensity of diffraction peaks increases with increasing calcination temperature, which indicates that degree of $LiMnPO_4$ crystallinity increases with increasing calcination temperature.

According to the Scherrer formula [27]: $D = K\lambda/(\beta\cos\theta)$, where D is crystallite diameter, $K = 0.89$ (the Scherrer constant), $\lambda = 0.15406$ nm (wavelength of the X-ray used), β is the width of line at the half-maximum intensity and θ is the corresponding angle. The resulting crystallite sizes of the products from calcined precursor at
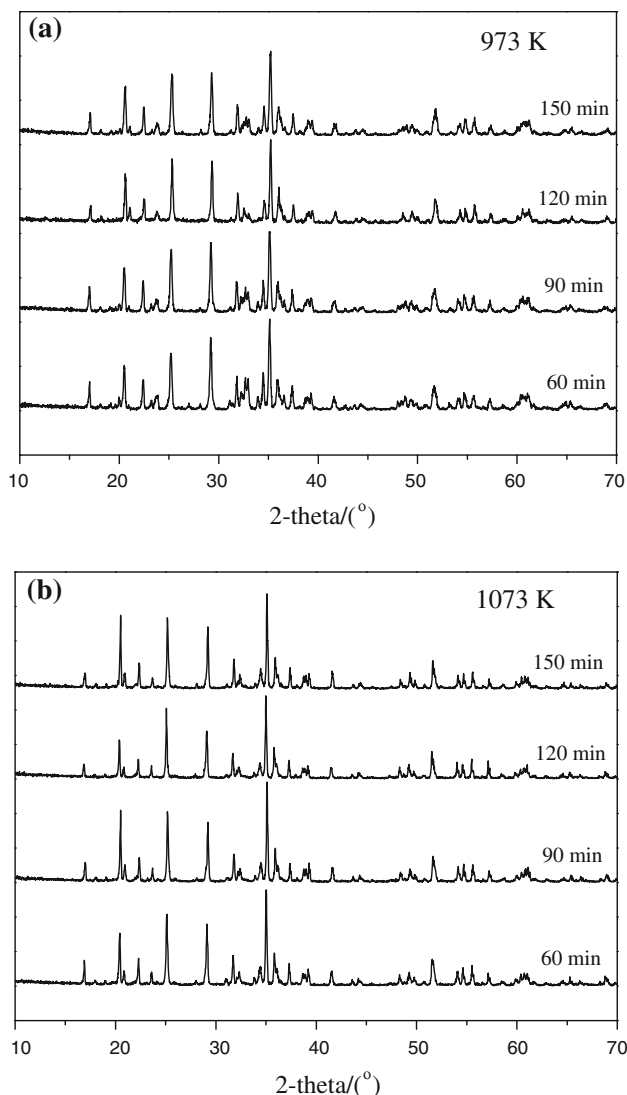

Fig. 2 FT-IR spectra of the precursor and its calcined products
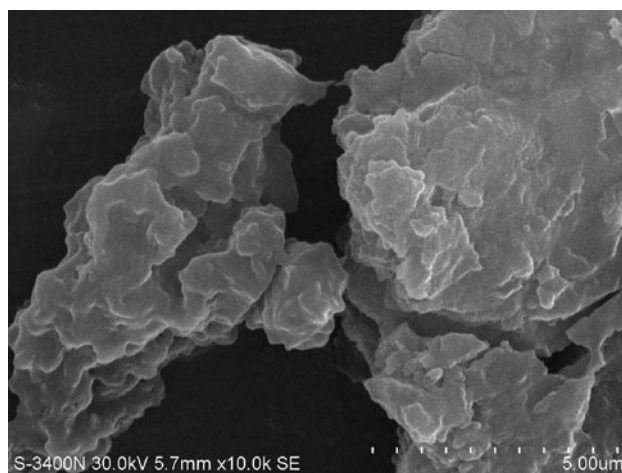
Fig. 4 SEM micrograph of $LiMnPO_4$ obtained at 973 K for 2 h

the temperatures of 773, 973, and 1073 K, are 29, 38, and 55 nm, respectively.

The morphology of LiMnPO$_4$ obtained at 973 K for 2 h is shown in Fig. 4. From Fig. 4, it can be seen that the LiMnPO$_4$ sample is composed of platelets. LiMnPO$_4$ sample illustrated polyhedral grains, which contains particles having a distribution of small particles (150–300 nm) and large particles (300 nm–2.0 μm). Its average crystallite size determined by X-ray diffraction is 38 nm, significantly smaller than the values determined by SEM. This is because observations by SEM technique give the size of the secondary particles, and the X-ray line broadening analysis disclosed the size of primary particles.

The XRD diffraction patterns for the powders isothermally calcined at 973, 1073 K for various periods of time are shown in Fig. 5a and b, respectively. From Fig. 5a and
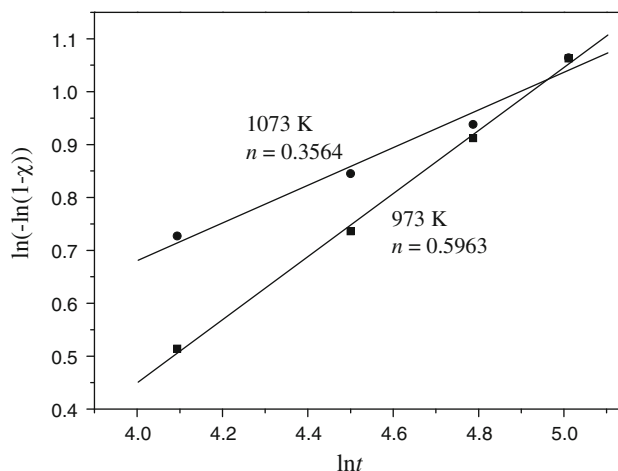
b, intensity of diffraction peaks increases with increasing calcination time, which indicates that degree of crystallization of LiMnPO$_4$ increases with increasing calcination times.

In accordance with XRD analysis in Fig. 5, the crystallized fraction of LiMnPO$_4$ at a given time t was calculated via MDI Jade 5.0 software at first, and then the plot of the crystallinity (χ) of LiMnPO$_4$ versus ln$t$ was plotted. The dependence of χ on ln$t$ is shown in Fig. 6, the result showed that the dependence of χ on ln$t$ gave a linear relation.

Figure 7 showed the dependence of ln[−ln(1−χ)] on ln$t$, it was found that the dependence of ln[−ln(1−χ)] on ln$t$ gave rise to a straight line. In accordance with JMA equation (Eq. 2), the slopes and intercepts of these straight lines can be determined, and then the rate constant (k), the Avrami exponent (n) were obtained, and the activation energy (E_c) of the crystallization process of LiMnPO$_4$ can

Fig. 5 XRD patterns of the products calcined for various periods of time
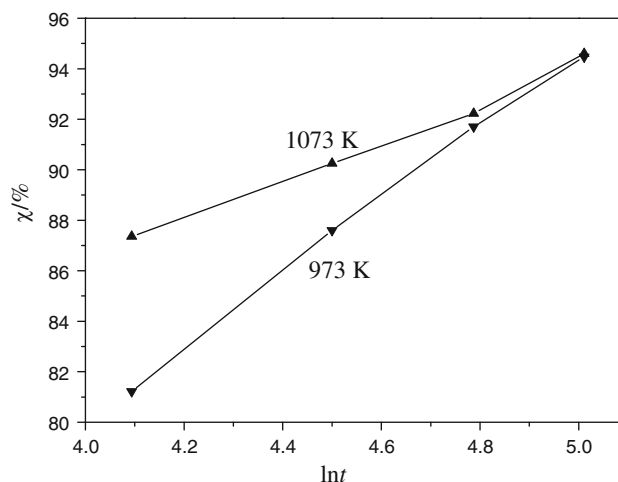
Fig. 6 Plots of the crystallinity (χ) of LiMnPO$_4$ versus ln$t$

Fig. 7 Plots of the ln(−ln(1−χ)) versus ln$t$

Table 1 The kinetic parameters of the crystallization process of $LiMnPO_4$

Temperature (K)	Rate constant (k)	Avrami exponent (n)	Activation energy (E_c, kJ/mol)
973	0.144	0.5963	
1073	0.475	0.3564	103.30

be obtained by Eq. 4. Table 1 showed the kinetic parameters of the crystallization process of $LiMnPO_4$.

The value of Avrami exponent (n) reflects the mechanism dominating the crystallization. Smaller n values indicate that the crystallization is dominated by a surface crystallization mechanism rather than by volume crystallization, and that the crystallization dimension is low. On the other hand, larger n values are expected only in case of increasing nucleation rates, i.e., $n > 2.5$ in diffusion-controlled reaction or $n > 4$ in polymorphic transformation [34]. For $LiMnPO_4$, the value of the Avrami exponent (n) was smaller than 1, which suggests that crystallization process of $LiMnPO_4$ is the random nucleation and growth of nuclei reaction [35, 36].

Conclusions

This research has successfully achieved a simple room temperature synthesis of orthorhombic $LiMnPO_4$. XRD analysis shows that orthorhombic $LiMnPO_4$ can be obtained via calcining its precursor at 973 K, and the crystallite size of the product is 38 nm. The activation energy of crystallization process for the $LiMnPO_4$ is 103.30 kJ/mol. The Avrami exponent, n, was smaller than 1, which suggests that crystallization process of $LiMnPO_4$ was the random nucleation and growth of nuclei reaction.

References

1. Valanarasu S, Chandramohan R (2010) J Mater Sci 45:2317. doi:10.1007/s10853-009-4195-z
2. Arai H, Tsuda M, Saito K, Hayashi M, Sakurai Y (2002) J Electrochem Soc 149:A401
3. Park BG, Kim S, Kim ID, Park YJ (2010) J Mater Sci 45:3947. doi:10.1007/s10853-010-4460-1
4. Xiang HF, Wang H, Chen CH, Ge XW, Guo S, Sun JH, Hu WQ (2009) J Power Sources 191:575
5. Wang Y, Jiang J, Dahn JR (2007) Electrochem Commun 9:2534
6. Padhi AK, Nanjundaswamy KS, Goodenough JB (1997) J Electrochem Soc 144:1188
7. Molenda J, Ojczyk W, Świerczek K, Zając W, Krok F, Dygas J, Liu RS (2006) Solid State Ionics 177:2617
8. Kobayashi G, Yamada A, Nishimura SI, Kanno R, Kobayashi Y, Seki S, Ohno Y, Miyashiro H (2009) J Power Sources 189:397
9. Molenda J, Ojczyk W, Marzec J (2007) J Power Sources 174:689
10. Choi D, Wang D, Bae IT, Xiao J, Nie Z, Wang W, Viswanathan VV, Lee YJ, Zhang JG, Graff GL, Yang Z, Liu J (2010) Nano Lett 10:2799
11. Drezen T, Kwon NH, Bowen P, Teerlinck I, Isono M, Exnar I (2007) J Power Sources 174:949
12. Yao J, Bewlay S, Konstantionv K, Drozd VA, Liu RS, Wang XL, Liu HK, Wang GX (2006) J Alloys Compd 425:362
13. Kim TR, Kim DH, Ryu HW, Moon JH, Lee JH, Boo S, Kim J (2007) J Phys Chem Solids 68:1203
14. Wang DY, Buqa H, Crouzet M, Deghenghi G, Drezen T, Exnar I, Kwon NH, Miners JH, Poletto L, Grätzel M (2009) J Power Sources 189:624
15. Chen GY, Richardson TJ (2010) J Power Sources 195:1221
16. Doan TNL, Bakenov Z, Taniguchi I (2010) Adv Powder Technol 21:187
17. Oh SM, Oh SW, Yoon CS, Scrosati B, Amine K, Sun YK (2010) Adv Funct Mater 20:3260
18. Xiao J, Xu W, Choi D, Zhang J (2010) J Electrochem Soc 157:A142
19. Yamada A, Hosoya M, Chung SC, Kudo Y, Hinokuma K, Liu KY, Nishi Y (2003) J Power Sources 119–121:232
20. Yang S, Zavalij PY, Whittingham MS (2001) Electrochem Commun 3:505
21. Prosini PP, Zanc D, Pasquali M (2001) Electrochim Acta 46:3517
22. Chen Z, Dahn JR (2002) J Electrochem Soc 149:A1184
23. Li G, Azuma H, Tohda M (2002) Electrochem Solid State Lett 5:135
24. Delacourt C, Poizot P, Morcrette M, Tarascon JM, Masquelier C (2004) Chem Mater 16:93
25. Wu WW, Li SS, Liao S, Xiang F, Wu XH (2010) Rare Metals 29:149
26. Avrami M (1939) J Chem Phys 7:1103
27. Avrami M (1940) J Chem Phys 8:212
28. Avrami M (1941) J Chem Phys 9:177
29. Vaish R, Varma KBR (2007) J Cryst Growth 307:477
30. Wu WW, Fan YJ, Wu XH, Liao S, Li SS (2009) J Phys Chem Solids 70:584
31. Koleva VG (2005) Spectrochimica Acta Part A 62:1196
32. Boonchom B, Danvirutai C, Maensiri S (2008) Mater Chem Phys 109:404
33. Boonchom B, Puttawong S (2010) Physica B 405:2350
34. Takei T, Kameshima Y, Yasumori A, Okada K (2001) J Eur Ceram Soc 21:2487
35. Johnson BR, Kriven WM, Schneider J (2001) J Eur Ceram Soc 21:2541
36. Boonchom B, Danvirutai C (2009) J Therm Anal Calorim 98:771